united nations
educational, scientific
and cultural
organization

international atomic
energy agency

the
abdus salam
international centre for theoretical physics

SMR/1270-14

SCHOOL ON SYNCHROTRON RADIATION

6 November – 8 December 2000

Miramare - Trieste, Italy

Supported in part by the Italian Ministry of Foreign Affairs in connection with the SESEME project

Co-sponsors: Sincrotrone Trieste, Società Italiana di Luce di Sincrotrone (SILS) and the Arab Fund for Economic and Social Development

Powder Diffraction

A. Benedetti & P. Canton
Università di Venezia
Italy

Powder Diffraction

Alvise Benedetti & Patrizia Canton

13th November 2000

Contents

1 Scattering by Policrystals and Amorphous Materials

1.1 Theory

This lesson is based on the References [1], [2], [3], [4], [5].

During World War I scientists in two different parts of the world indipendently discovered that there existed a characteristic x-ray diffraction effect from a fine-grained crystalline aggregate. This discovery was made by Debye and Scherrer in Germany and almost simultaneously by Hull in the United States.

Although much information is lost or degraded by using an aggregate in place of a single crystal, this method of investigating crystal has proved to be exceedingly useful in those cases where single crystals are not available, are difficult to obtain or one wishes to examine a crystalline material which is not in the form of discrete single crystal, for example, a metal. There are many applications of the powder method, but two of these are of primary importance. Fundamentally, the powder method provides a way of investigating, within limits, the crystallography of the crystal in the powder. Secondarily, since the powder diffraction diagram produced by a crystalline substance is a characteristic of that substance, the powder method can be used as a means of identification of crystal.

Each crystal may be envisaged as a reciprocal lattice. Since an ideal policrystalline material or powder is an ensemble of a very large number of randomly oriented crystallites, the reciprocal lattices associated with them are randomly oriented also. The origin of all these lattices, however, lie at the point where the direct beam leaves the sphere of reflection.

Consider the reciprocal-lattice point *hkl* at the end of the vector σ_{hkl} in Fig. 1. If there is an infinite number of crystals in the powder,there must be an

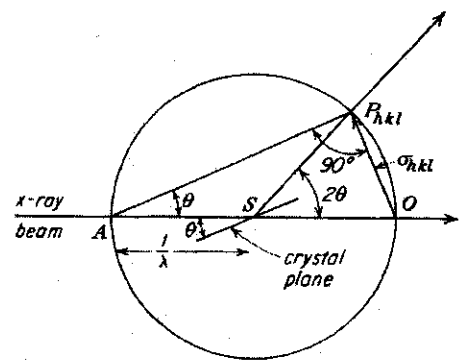

Figure 1: [1].

infinite number of such points *hkl*, all lying at a vector distance σ_{hkl} from the origin. Since these vectors are randomly directed in space, the reciprocal-lattice points *hkl* must lie on a sphere centred at the origin.
This is obviously true of any reciprocal-lattice point *hkl*. The sum total of all reciprocal-lattice points, therefore, comprises a set of concentric spheres of radii σ_{hkl} centered at an origin which lies on the sphere of reflection. These reciprocal-lattice spheres, therefore, intersect the sphere of reflection in small circles. Since a diffracted beam develops whenever a reciprocal-lattice point intersects the sphere of reflection, the diffracted beams form cones emanating from the center of the sphere of reflection, as illustrated in Fig.2 for one such cone.

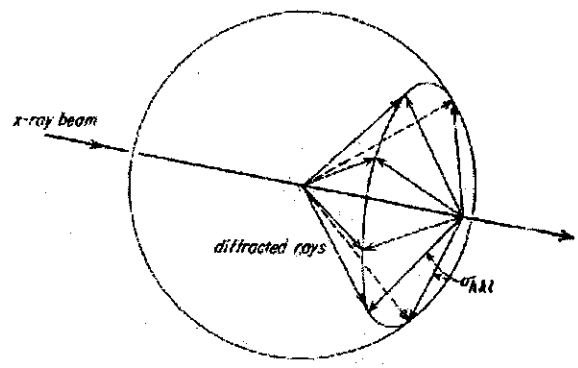

Figure 2: [1].

The principles involved in the production of a powder diagram can be appreciated by considering the simplified experimental arrangement shown in Fig.3. An X-ray beam is defined by the pinhole system, just described. A photographic film is then placed normal to the x-ray beam. The powder sample is introduced into the path of the x-ray beam. As the beam travels through the powder sample, it meets thousands of powder grains, each a tiny crystal in a different orientation.
Among these grains many are so oriented that a particular set of planes *hkl* makes the appropriate glancing angle θ (for the plane) with the x-ray beam. Such grains are in the position to reflect X-rays. The reflection occurs in a direction making an angle 2θ with the direct x-ray beam. The locus of directions making an angle 2θ with a given direction is a cone of half opening angle 2θ. For each solution of the Bragg equation

$$\theta = \sin^{-1}\left(\frac{\lambda \cdot n}{2 \cdot d_{hkl}}\right) \tag{1}$$

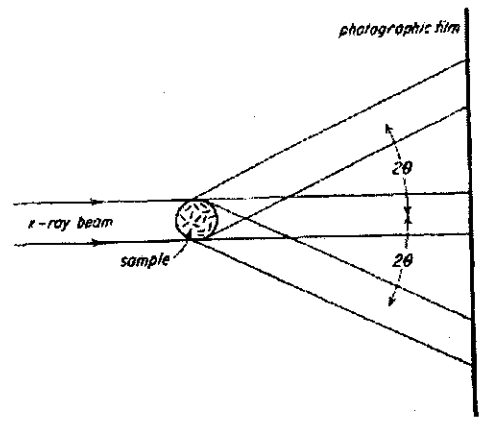

Figure 3: [1].

there exists such a cone.
We remember that in a space lattice each Miller index triplet is represented by a series of parallel equispaced planes containing all the lattice points. In actual crystals these planes are the loci of the atomic or molecular units of the crystal pattern. d_{hkl}, the interplanar spacing, is the perpendicular distance between successive planes of a series.

A simply way to record the diffraction pattern of a policrystalline material is by placing a film perpendicular to the incident X-ray beam. The diffraction cones will, in this case, give rise to a series of concentric rings each satisfying the Bragg law (Fig. 4).

Alternatively, a narrow strip of film can be placed on the cylinder centred on the sample. In this case, the cones will generate concentric arcs, which are segments of the rings, on the strip (Fig. 5).

A final possibility is to reduce the strip to a line, that is simply to record the position and the intensity of the diffracted radiation on any plane that contains the incident X-ray beam. In this last case, one only measures the radius of the cone and the diffracted intensity at a single position. If the sample can be considered perfectly isotropic this single measurement is sufficient to completely characterize the diffraction pattern. The parameters reported are 2θ, that is the angle made by any vector with origin in A (see Fig. 2) and lying on the diffraction cone surface and the incident X-ray beam, and the relative intensity of the radiation along any direction on the cone (Fig. 6).

Let us consider now, a diffracting object in which the relative positions of the atoms are fixed. We assume that the object rotates in such a manner that all possible orientations with respect to the incident beam are equally probable. We also assume that this motion is sufficently rapid so that one observes only

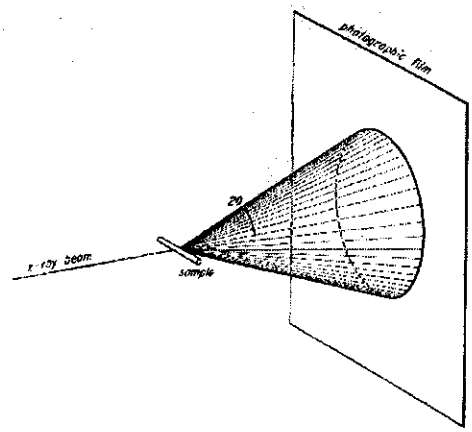

Figure 4: [1].

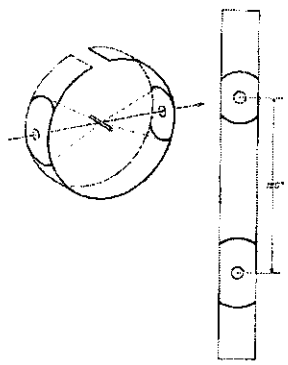

Figure 5: [1].

the average diffracted intensity. This is equivalent to observing the diffraction by a collection of identical objects with random orientations and positions. We shall call such object a perfect powder.

The Debye formula for the intensity is

$$I = \sum_m \sum_n f_m f_n \frac{\sin(hr_{mn})}{hr_{mn}} \tag{2}$$

Let us consider an object composed of atoms or of identical group of atoms with structure factor F. We consider first in Eq. (2) the N terms related to a given atom, and we notice that each pair is counted twice, the distance r_{mn} being equal to r_{nm}. We shall call r_z the interatomic distances in the object. There

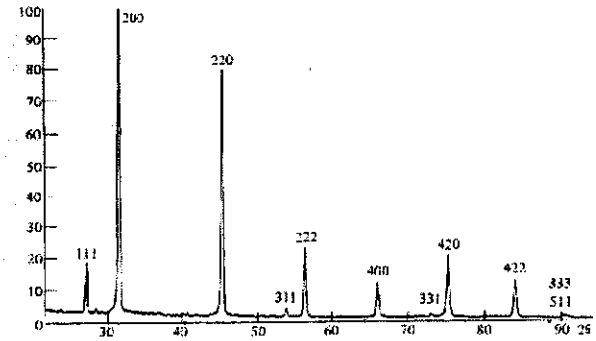

Figure 6: [2].

are $[N(N-1)]/2$ of these. According to the Debye formula the interference function is

$$F(h) = \frac{I}{NF^2} = 1 + \frac{2}{N}\sum_z \frac{\sin(hr_z)}{hr_z} \tag{3}$$

The powder diagram depends only on the lengths of all the interatomic vectors, it does not depend on their mutual orientations.

The Debye formula applies, in particular to a crystalline powder of identical particles. Let us consider grains of a simple cubic crystal having the form of cubes measuring $(n-1)a$, a being the lattice parameter of the unit cell. The scattering power is

$$F(h) = 1 + \frac{6n^2(n-1)}{n^3}\frac{\sin(ha)}{ha} + \frac{12n(n-1)^2}{n^3}\frac{\sin(ha)\sqrt{2}}{ha\sqrt{2}} \tag{4}$$

This equation gives the intensity of the Debye-Scherrer powder diagram, taking into account the shapes of the lines due to the size of the elementary crystal. It is not obvious from this equation that the intensity is zero everywhere, except in the immediate neighbourhood of the lines corresponding to the Bragg angles. A complex calculation shows, however, that this expression is equivalent to that derived from the classical expression valids for a small crystall having the shape of a parallelopipedon with edges N_1a_1, N_2a_2, N_3a_3 parallel to the crystal axes $\boldsymbol{a_1}\boldsymbol{a_2}\boldsymbol{a_3}$:

$$I = I_e F^2 \frac{\sin^2[(\pi/\lambda)(\boldsymbol{s}-\boldsymbol{s_0})\cdot N_1\boldsymbol{a_1}]}{\sin^2[(\pi/\lambda)(\boldsymbol{s}-\boldsymbol{s_0})\cdot \boldsymbol{a_1}]} \frac{\sin^2[(\pi/\lambda)(\boldsymbol{s}-\boldsymbol{s_0})\cdot N_2\boldsymbol{a_2}]}{\sin^2[(\pi/\lambda)(\boldsymbol{s}-\boldsymbol{s_0})\cdot \boldsymbol{a_2}]} \frac{\sin^2[(\pi/\lambda)(\boldsymbol{s}-\boldsymbol{s_0})\cdot N_3\boldsymbol{a_3}]}{\sin^2[(\pi/\lambda)(\boldsymbol{s}-\boldsymbol{s_0})\cdot \boldsymbol{a_3}]} \tag{5}$$

where

$$\left|\frac{\boldsymbol{s}-\boldsymbol{s_0}}{\lambda}\right| = \frac{2\sin\theta}{\lambda}$$

$y = (\sin^2 Nx)/\sin^2 x$ is a peak function essentially zero everywhere except in the immediate vicinity of $x = n\pi$ where it rises to high maxima and the peaks are, accordingly, higher and sharper when N increases. Hence the intensity, I, will be essentially zero unless the three quotients are simultaneously close to their maximum values. For I to be a maximum, we must simultaneously satisfy the three conditions

$$(\pi/\lambda)(s - s_0) \cdot a_1 = h'\pi$$
$$(\pi/\lambda)(s - s_0) \cdot a_2 = k'\pi$$
$$(\pi/\lambda)(s - s_0) \cdot a_3 = l'\pi$$

where h', k', l' are three integers. Rearranged and written in the form below, these are called the three Laue equations:

$$\begin{aligned} (s - s_0) \cdot a_1 &= h'\lambda \\ (s - s_0) \cdot a_2 &= k'\lambda \\ (s - s_0) \cdot a_3 &= l'\lambda \end{aligned} \tag{6}$$

Since a diffracted beam exists only if the three Laue equations are simultaneously satisfied, the three equations together must be equivalent to the Bragg law.

In the powder method, a monochromatic beam falls upon a powder sample containing an enormous number of very small crystals having completely random orientations. For any set of planes hkl with spacing d_{hkl}, there will be a few crystals whose planes hkl make the correct angle with the primary beam to allow a Bragg reflection such that the corresponding powder pattern shows a sequence of line profile characteristic of the crystalline system investigated.

1.2 Line Broadening Analysis

Esperimentally a diffraction line profile is the result of the convolution of a number of independent contributing shapes, some symmetric and some asymmetric. It can be represented as:

$$h(x) = \int g(x')f(x - x')dx' + background = g(x) * f(x) + background$$

where x measures the angular deviation of any point from the theoretical scattering angle $2\theta_0$, x' is the variable of integration in the same x domain, g(x) is the instrumental profile function, f(x) is the intrisic diffraction profile function, and h(x) is the resulting observed profile function.
Recently powder profile refinement methods devoted

1) to deriving structural parameters such as atomic coordinates in the unit cell, thermal motion etc.
2) to extract physical information such as: phase identification, crystallite size, lattice disorder

have been developed. In order to describe the experimental profiles, symmetric analytical profile functions such as: Gaussian, Lorentzian, pseudo-Voigt, Pearson VII etc. have been used.

Eq.5 can be used to show the effect on the diffraction pattern of various crystal imperfections such as small crystallite size, strains and faulting. Since it is the simplest kind of imperfection we shall deal mostly with the effect of small crystallite size remembering that the diffraction line becomes broader as the crystal size decreases.

The first treatment of particle size broadening was due to Scherrer.
He showed that

$$L = \frac{K\lambda}{B(2\theta)\cos\theta} \tag{7}$$

wherein θ and λ have their usual meaning, L is the mean dimension of the crystallites composing the powder, $B(2\theta)$ is the full width in radians subtended by the half maximum intensity width of the powder pattern peak, and K a costant approximately equal to unity and related to the crystalline shape.

A more general treatment was proposed by Warren and Averbach (Fourier method) in which some information about strains can also be provided. It can be summarized as follows:
the experimental broadened profile has to be deconvoluted from the instrumental and spectral effects in order to obtain the corrected Fourier transforms A(L) (L is the variable in the direct space). According to Warren and Averbach the coefficients A(L) (or the Fourier transforms) are the products of size coefficients $A_s(L)$ and distortion coefficients $A_d(L)$:

$$A(L) = A_s(L)A_d(L) \tag{8}$$

where $A_s(L)$ is indipendent of the peak order and $A_d(L)$ is dependent upon the order of the diffraction peak. If at least two orders of reflections of the same plane family are known, by means of the following expression:

$$\ln A\left(L, \frac{1}{d_{hkl}^2}\right) = \ln A_s(L) - 2\pi^2 < \epsilon^2(L) > \frac{L^2}{d_{hkl}^2} \tag{9}$$

where hkl are the Miller indices, $< \epsilon^2(L) >$ is the squared microstrain averaged over all distances L, and d_{hkl} is the interplanar spacing, it is possible to separate the crystalline size contribution from that of lattice distortion.

1.3 Amorphous Materials

For very small cluster containing few atoms it is preferable to calculate the pattern from the Debye formula. If we consider a liquid, it has no structure with respect to a fixed origin since the atoms are continually moving about. In an amorphous solid (glasses, glassy metals, resins, unoriented solid polymers), the atoms have permanent neighbours but there is no repeating structure, only local configurations. Although there is no sharp dividing line between crystalline and the so called amorphous materials, for clarity in this discussion we somewhat

arbitrarily designate as *crystalline* those materials characterized by three dimensional periodicity over appreciable distances, say, of the order of six or more unit translations. Conversely, materials possesing only one or two-dimensional, or lesser, degrees of order are referred to as *amorphous.*

Fig. 7 is a two dimensional illustration of the difference between the arrangement of atoms in a hypothetical crystal A and glass B of the same chemical composition, A_2O_3.

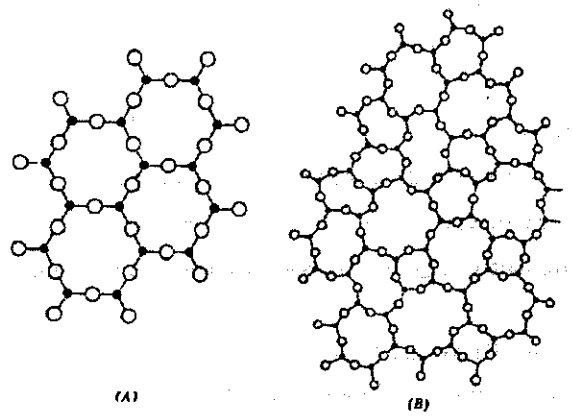

Figure 7: [3].

However, atoms have well-defined sizes and closest distances of approach, and hence both liquids and amorphous solids have definite structures relative to an origin at the center of an average atom. This type of structure is expressed by a Radial Distribution Function (RDF) $4\pi r^2\rho(r)$ such that $4\pi r^2\rho(r)dr$ is the average number of atom centres between distances r and $r+dr$ from the center of an average atom.

Eq. (2) makes it possible to estabilish the correct atomic configuration by inverting the experimental intensity function by means of the Fourier integral theorem as first suggested by Zernike and Prins, and so to obtain the RDF of the specimen.

The application of the Fourier integral theorem is perfectly straightforward in the case of a substance consisting of only one kind of atom. Then Eq. (2) becomes

$$I = Nf^2 \sum_m \frac{\sin(hr_{mn})}{hr_{mn}} \tag{10}$$

if it is assumed that the enviroment of one atom is the same as that of any other atom.

Since in performing the summation of eq. (10) each atom in turn becomes the reference atom, there are N terms due to the interaction of each atom with

itself. The value of each of these terms is unity, since in the limit as $r_{mn} \to 0$, $\frac{\sin(hr_{mn})}{hr_{mn}}) \to 1$. So eq. (10) may be written

$$I = Nf^2 \left(1 + \sum_m \frac{\sin(hr_{mn})}{hr_{mn}}\right) \tag{11}$$

if it be understood that the summation excludes the origin atom. The distribution of atoms about any reference atom may now be regarded as a continuous function and the summation replaced by an integral

$$I = Nf^2 \left[1 + \int_0^\infty 4\pi\rho(r)\frac{\sin(hr)}{hr}\, dr\right] \tag{12}$$

Here $\rho(r)$ is the number of atoms per unit volume at a distance r from the reference atom, and $4\pi r^2\rho(r)dr$, as reported above, is the number of atoms contained in a spherical shell of radius r and thickness dr. Letting ρ_0 be the average density of atoms in the sample, eq.(12) may be rewritten as

$$I = Nf^2 \left\{1 + \int_0^\infty 4\pi r^2 \left[\rho(r) - \rho_0\right]\frac{\sin(hr)}{hr}\, dr + \int_0^\infty 4\pi r^2\rho_0\frac{\sin(hr)}{hr}\, dr\right\} \tag{13}$$

The integral of the last term of eq.(13) represents the scattering by a hypothetical object of the same form as the specimen but of rigorously uniform electron density. This is the central scattering, which occurs at such small angles as to be unresolvable from the direct beam. Hence, if attention is limited to experimentally observable intensities, i(h), eq.(13) can be simplified to the form

$$\frac{I}{Nf^2} - 1 = \int_0^\infty 4\pi r^2\left[\rho(r) - \rho_0\right]\frac{\sin(hr)}{hr}\, dr$$

By means of the Fourier integral theorem, this expression can be transformed to

$$r\left[\rho(r) - \rho_0\right] = \frac{1}{2\pi^2}\int_0^\infty hi(h)\sin(hr)\, dh$$

$$4\pi r^2\rho(r) = 4\pi r^2\rho_0 + \frac{2r}{\pi}\int_0^\infty hi(h)\sin(hr)\, dh$$

where

$$i(h) = \frac{I}{Nf^2} - 1$$

The case of the presence of more than one kind of atom will be treated in section 2.

1.4 Rietveld Method

This lesson is based on the Reference [6].

In these last years, dedicated powder diffractometers are in operation at many synchrotron sources. In contrast to conventional radaition source, the main properties of synchrotron radiation are

1) the extremely good instrumental resolution over extended angular ranges (for example, full widths at half maximum of $< 0.01^o$ out to a d-spacing of 1Å at a wavelength of 0.7Å),
2) excellent peak-to-background discrimination,
3) peak shapes which are very well described by the commonly-used pseudo-Voigt function (including a simple and reliable asymmetry correction for axial divergence at lower angle),
4) high brightness (large amount of flux in a well collimated beam)
5) an intense continuos wavelength distribution spectrum, for which monchromatized X-radiation can be selected and the consequent possibility of using anomalous scattering as a general probe of cation distribution for elements with Z>35.

As an example Fig.8 shows the variation in instrument-only contributions to the peak full width at half maximum (FWHM) as a function of diffraction angle for a number of modern neutron and X-ray diffractometers.

In this part, some of the most important aspects will be treated in relation to their applications in Material Science. In particular, beside some general considerations on the application of the broadening analysis and kinetics of crystallization, the Rietveld method, thin films analysis, anomalous scattering and their relative applications will be briefly reported.

In the mid-sixties, it became apparent to various diffractionists that much more information could be obtained from a powder pattern if the full power of computers could be applied to full-pattern analysis. The recognized point was that in a step-scanned pattern, for example, there was some information attached to each intensity at each step in the pattern, even if it were the negative information that there was no Bragg-reflection intensity there or the partial and the scrambled information that the intensity at a step was the sum of contributions from the details of several Bragg reflections. It was Rietveld who first worked out computer-based analytical procedures to make use of the full information content of the powder pattern.

In the Rietveld method the least-squares refinements are carried out until the best fit is obtained between the entire observed powder diffraction pattern taken as a whole and the entire calculated pattern based on the simultaneously refined models for the crystal structure(s), diffraction optics effects, instrumental factors, and other specimen characteristics (e.g. lattice parameters) as may be desired and can be modelled.

A powder diffraction pattern of a crystalline material may be thought of as a collection of individual reflection profiles, each of which has a peak height, a peak

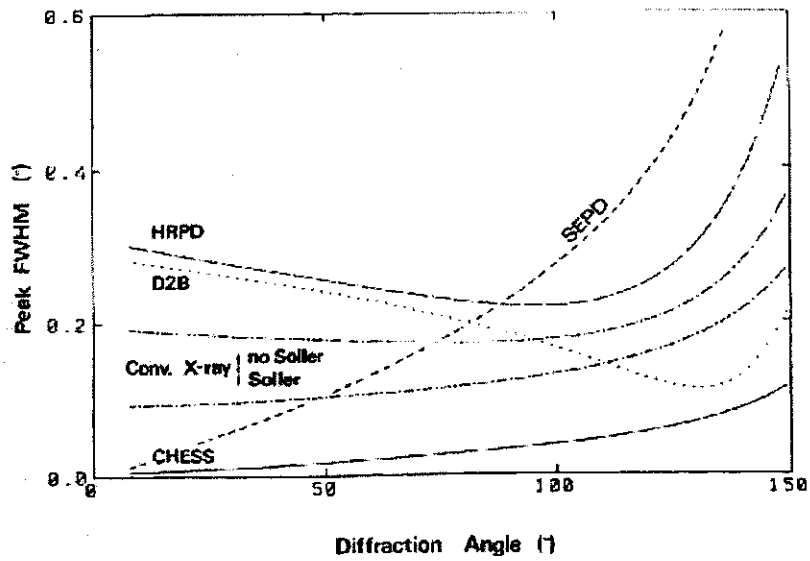

Figure 8: Variation in the instrumental-only peak FWHM as a function of diffraction angle (2θ) for several neutron and X-ray diffractometers. The curves represent the following instruments: long – – HRPD (CW neutron) at Lucas Heights; ··· D2B (CW neutron) at the ILL; short - - SEPD (TOF neutron) at the ANL; -.-.- conventional (X-ray) Bragg-Brentano with (lower) and without (upper) diffracted-beam Soller slits; —— synchrotron (X-ray) Bragg-Brentano at CHEES [6].

position, a breadth, tails which decay gradually with distance from the peak position, and an integrated area which is proportional to the Bragg intensity, I_K, where K stands for the Miller indices, h, k, l. I_K is proportional to the square of the absolute value of the structure factor, F_K^2. In all powder diffraction patterns but those so simple that the Rietveld method is not needed in the first place, these profiles are not all resolved but partially overlap one another to a subtantial degree.

If y_i is the numerical intensity value recorded at each of equal increments (steps),i, in the pattern the quantity minimized in the least-squares refinement is the residual, S_y:

$$S_y = \sum_i w_i(y_i - y_{ci})^2$$

where $w_i = 1/y_i$; y_i =observed intensity at the ith step; y_{ci} =calculated intensity at the ith step, and the sum is overall data points. It is a crucial feature of the Rietveld method that no effort is made in advance to allocate observed

intensity to particular Bragg reflections nor to resolve overlapped reflections. Consequently, a reasonably good starting model is needed. The method is a structure refinement method. Typically, many Bragg reflections contribute to the intensity, y_i, observed at any arbitrary chosen point, i, in the pattern. The calculated intensities y_{ci} are determined from the values calculated from the structural model by summing of the calculated contributions from neighbouring (i.e. within a specified range) Bragg reflections plus the background:

$$y_{ci} = s \sum_K L_K |F_K|^2 \phi(2\theta_i - 2\theta_K) P_K A + y_{bi}$$

where

s is the scale factor,
K represents the Miller indices, *hkl*, for a Bragg reflections,
L_K contains the Lorentz, polarization, and multiplicity factors,
ϕ is the reflection profile function,
P_K is the preferred orientation function,
A is the absorption factor,
F_K is the structure factor for the Kth Bragg reflection, and
y_{bi} is the background intensity at the ith step.

The usual refinable parameters are listed as follow:

For each phase present

- x_i, y_i, z_i, B_i, N_i (x_i, y_i and z_i are position coordinates, B_i is an isotropic thermal parameter, and N_i is the site-occupancy multiplier, all for the ith atom in the unit cell)
- Scale factor (note quantitative phase analysis possibility)
- Specimen-profile breadth parameters
- Lattice parameters
- Overall temperature factor (thermal parameter)
- Individual anisotropic thermal parameters
- Preferred orientation
- Crystalline size and microstrain (through profile parameters)

Global parameters

- 2θ-Zero
- Instrumental profile

- Profile asymmetry
- Background
- Wavelength
- Specimen displacement
- Specimen transparency
- Absorption.

As an example, in Fig. 9 the final fitted profile of Lithium Disilicate, using Pearson VII functions, is reported

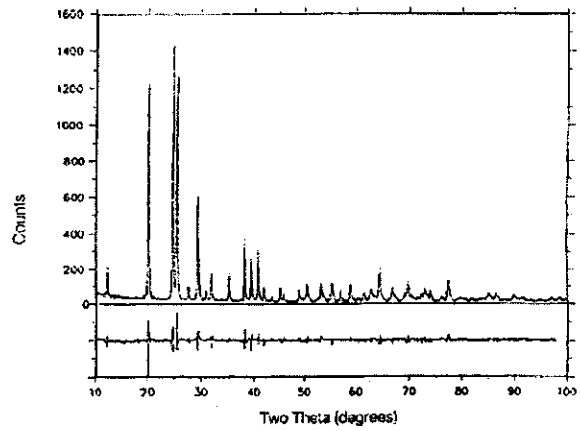

Figure 9: [7].

In the presence of multiple phases, Rietveld analysis can provide very accurate estimates of the relative and/or absolute abundaces of the component phases according to

$$W_p = \frac{S_p(ZMV)}{\sum_{i=1}^{n} S_i(ZMV)}$$

where W is the realtive weight fraction of phase p in a mixture of n phases; S, Z, M and V are, respectively, the Rietveld scale factor, the number of formula units per unit cell, the mass of the formula unit (in atomic mass units) and the unit cell volume (in $\AA^3$).

1.5 Thin Film

This lesson is based on the References [8], [9].

X-ray diffraction methods are widely used for the characterization of thin films. The increasing use of thin films with special tailored properties, for example for electronic devices, has stimulated the need for improved characterization methods. The properties are determined by the thin-film material and its crystal structure. The microstructure is critically dependent on the various parameters used in the deposition of the film, and their effect on the required properties can be followed by x-ray diffraction. It is well known that thin films are usually not uniform, and indeed it may be desiderable to purposely vary the microstructure as a function of the thickness to obtain the desired properties. Methods that obtain diffraction patterns from different film depths are now essential for complete structural characterization. The high intensity of a Synchrotron radiation is an important factor in measuring the weak scattering from thin films.

1.5.1 Reflection Geometry

In the microstructural analyses of thin films, special experimental techniques have to be employed to obtain diffraction patterns with sufficient statistical accuracy in a reasonable counting time. Since films and coatings are normally supported by a relatively thick substrate, one is forced to use the reflection geometry, shown in Fig.10.

In any case, the conventional x-ray methods, when used for thin films, the x-ray beam usually penetrates the entire film making it impossible to follow structural variations as a function of film depth.

The depth of x-ray penetration into the film depends on the angle of incidence α. When the incident angle becomes $<$ than a certain angle α_c, specific of the material, the depth is very small (usually about 50-100Å). The critical angle α_c for the total reflection is given by

$$\alpha_c = (2\delta)^{1/2} = 1.6 \cdot 10^{-3}\rho\lambda$$

where α_c is in radians, ρ is the density in gcc^{-1} and λ is the wavelength in Å. This ignores anomalous dispersion, which has a significant effect even on the long wavelength side of the absorption edge.

For $\alpha < \alpha_c$ the penetration depth t' is determined by the total external reflection process and is given by

$$t' = \frac{\lambda}{[2\pi(\alpha_c^2 - \alpha^2)^{1/2}]} \tag{14}$$

The thinnest layer that can be sampled is determined by the density of the film. For $\alpha > \alpha_c$ the penetration depth is dependent on the linear absorption coefficient μ_1:

$$t' = 2\alpha/\mu_1 \tag{15}$$

Fig. 11 shows the penetration depth in the iron oxide film as a function of α and λ as calculated by eqs. 14 and 15.

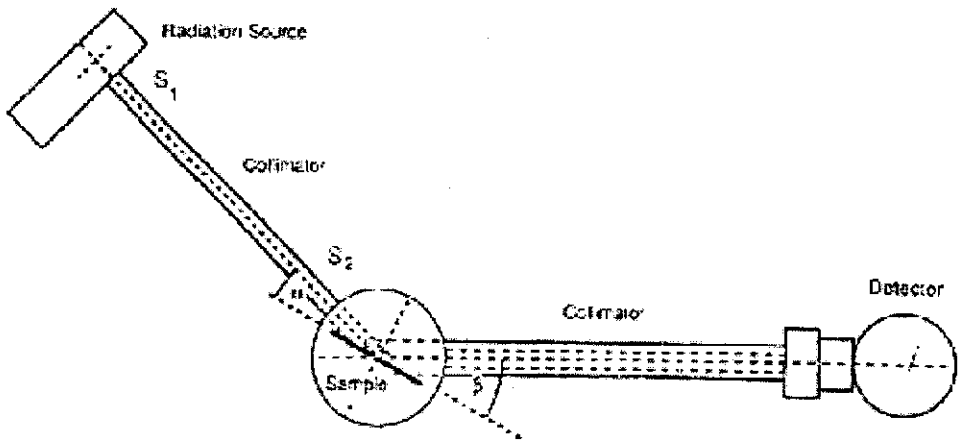

Figure 10: Reflection geometry with parallel X-ray beam, defined by the incident beam slits S_1 and S_2. In the fixed incidence: 2θ scanning, the sample surface makes a fixed angle α with the direction of the incident beam. The detector sees the same sample area at any angle of reflection β. The scattering angle is defined as $2\theta = \alpha + \beta$. In $\theta : 2\theta$ scanning, the angle of incidence $\alpha = \beta$ and the sample continuously bisects the angle 2θ, so that $\beta = \theta$ [8].

1.5.2 Seemann-Bohlin Geometry

For many years, researchers have employed the Seemann-Bohlin geometry (see Fig.12) for the measurements of the powder patterns of thin films. In the Seeman-Bohlin focusing geometry, the specimen is set at a fixed small angle (about 5° minimum) and the detector is moved around the focusing circle by a special linkage. However mechanical restriction prevents using smaller angle required for grazing incidence and any departure from the strict focusing requirements causes large geometrical aberration in the pattern.

1.5.3 Parallel Beam reflection geometry

Because of the limitations of the Seeman Bohlin geometry, it might be advantageous to adopt the parallel beam geometry with a fixed angle of incidence α (in Fig.13 θ_s) as shown in Fig.13. Since the specimen has a finite dimension, say 30 mm in width, one must limit the width of the primary beam to 1 mm in order to reach a low incidence angle $\alpha = 2°$. In this case, the detector is

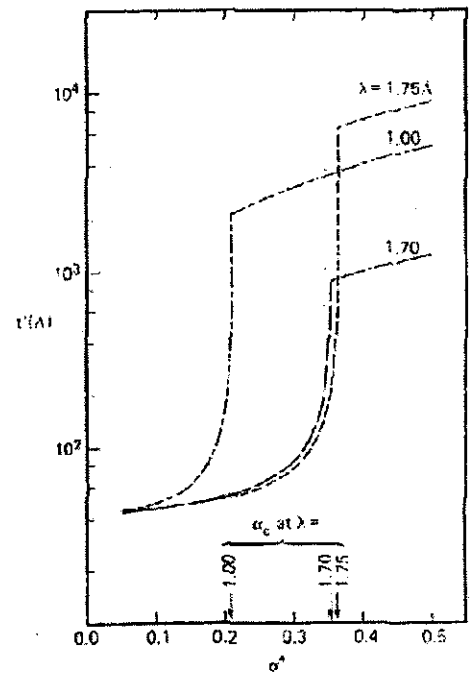

Figure 11: [9].

always looking at the entire irradiated area, and one must install a set of Soller slits whose blades are placed perpendicular to the diffraction plane so that the diffraction angle is well defined.

1.5.4 Grazing Incidence Scattering

As shown above, if one whishes to employ the effect of total reflection of the incident beam for the analysis of angstrom thick layers, one must reduce the angle of incidence α to a value less than the critical angle α_c which is only a fraction of one degree. Thus, the method of grazing incidence scattering (or diffraction) requires a very narrow x-ray beam because of the finite sample size and a strong primary beam, available with synchrotron sources. In this technique, one can scan the diffracted beam in the same way as presented in Fig.10, with the diffraction plane, containing the incident and diffracted beams, perpendicular to the specimen surface (method 1), i.e., using the parallel beam geometry.

One can also scan the diffracted beam almost parallel to the specimen surface as shown in Fig.14, i.e., the incident beam $I_{incident}$ strikes the specimen at

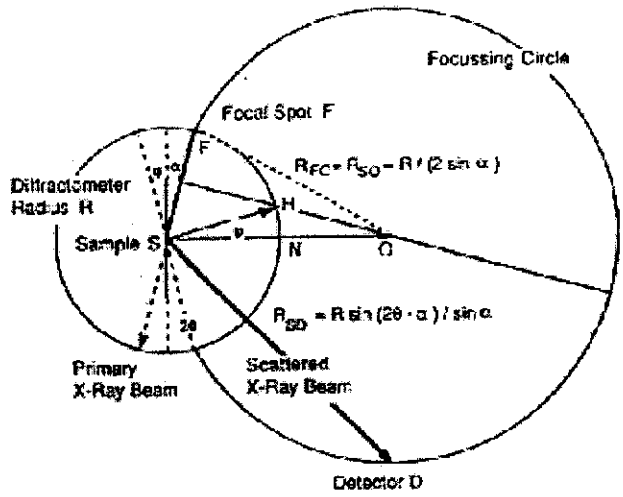

Figure 12: Focussing Seeman-Bohlin diffractometer. The sample S remains fixed at constant angle of incidence α, while the detector slit moves along SD by the amount $R_{SD} = R\sin(2\theta - \alpha)/\sin\alpha$ to remain on the focussing circle of radius $R_{FO} = R_{SO} = R/(2\sin\alpha)$, where R is the radius of the diffractometer. [8]

an angle $\alpha_i < \alpha_c$, and the diffracted beam is detected at a second grazing angle α_f. The diffraction angle 2θ is defined as the angle between the projections of α_i and α_f onto the specimen surface (method 2). As an example in Fig.15 are reported the grazing incidence diffraction profiles, $\alpha = 0.25°$, $\lambda = 1.75$, of unbroadened Si(111) powder and broadened 6.5h annealed iron oxide film (111): peak intensities normalized. Outer profile fitted with symmetrical Lorentz function.

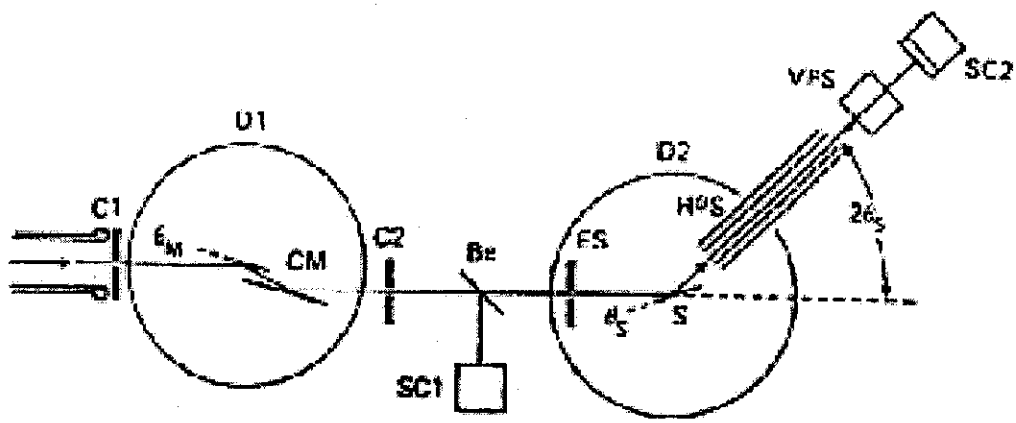

Figure 13: Parallel beam X-ray optics used in $\theta : 2\theta$ and grazing incidence: 2θ scanning. [9]

2 Anomalous X-ray Scattering

This lesson is based on the References [10], [11].

Even if the usefulness of the anomalous X-ray scattering has also been confirmed in structural investigation of polycrystalline samples (some examples will be reported during the lecture), we focalize our attention in *Amorphous Materials* (in which the atomic arrangement is not spatially periodic) containing more than two kinds of atoms in order to evaluate the partial radial distribution function.

The diffraction pattern from an amorphous sample (i.e. a glass) exhibits broad features, indicating the lack of translational symmetry in its structure. The quantity obtained from a conventional scattering experiment is the **radial distribution function** (RDF), which is a description of the average environment of an atom, for example, in a glass. The RDF is defined as $4\pi r^2\rho(r)$, where $\rho(r)$ is the radial density function and r is the radius; $\rho(r)$ is the average number density of atoms at a distance r from an average atom at the origin. The RDF, therefore, is the number of atoms in a shell of unit thickness at a distance r. The number of neighbours coordinating a central atom is obtained by integrating a peak in the RDF, and the average distance of these neighbours is obtained from the peak position.

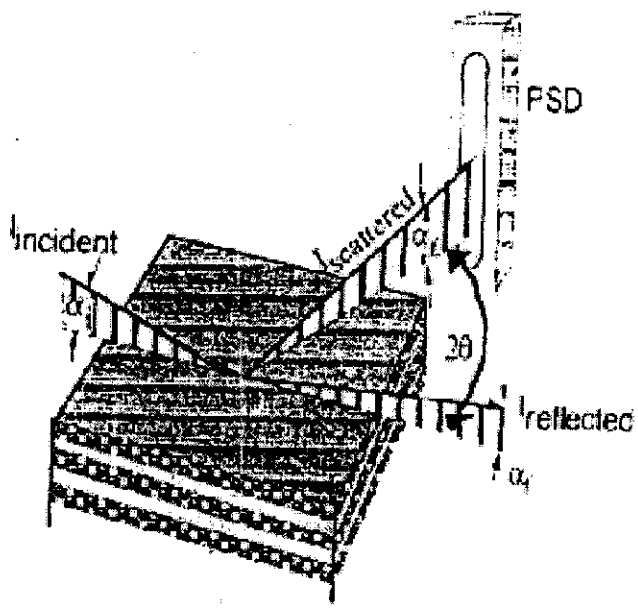

Figure 14: Schematic diagram showing grazing incidence scattering X-ray diffraction.

Even in one-component system, the interpretation of the RDF is difficult because the local structure is spherically averaged. In a multicomponent system, the problem is even more complex because the average environment portrayed by the RDF might bear little resemblance to the actual environment of any given component. Anomalous scattering experiments permit species-specific distribution functions to be obtained, which give a more direct view of the amorphous structure (such structural information is very similar to the results by EXAFS measurements).

When the X-ray energy is close to an absorption edge of an atom, the X-ray scattering factor changes significantly through the **anomalous scattering factors** (ASF's) f' and f''. For example, the scattering factor of Se is reduced from its maximum value by approximately 10 electrons at the K absorption edge energy. Therefore, Se (atomic number Z=34) scatters more like Cr (Z=24). Suppose scattering patterns are obtained from an Ag-Ge-Se glass at two X-ray energies close to the Se K absorption edge. The scattering behaviour of Se is different at each energy, but the behaviour of Ge and Ag is the same. The

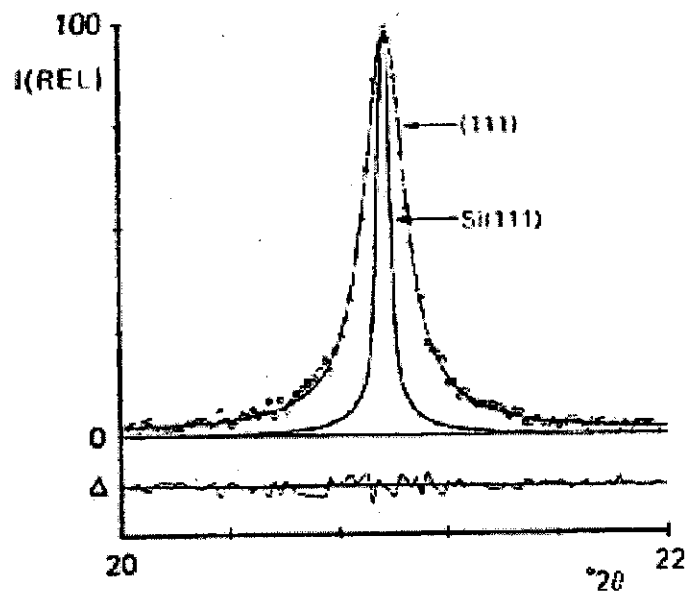

Figure 15: .[9]

difference between the two patterns can be related to the distance correlations involving Se atoms. The result of this type of experiment is the **difference distribution function** (DDF) around Se. The DDF is $4\pi r^2 \rho_{Se}(r)$, where $\rho_{Se}(r)$ is the density of atoms at a distance r from a central Se atom.

The idea of obtaining structural information from the derivative of the scattered X-ray intensity with respect to energy was first proposed by Shevchik [12], [13]. However, the **differential anomalous techniques** (DAS) technique outlined above was first developed and applied experimentally to amorphous $GeSe$ and glassy $GeSe_2$ by Fuoss [14], [15] Because the X-ray energy must be near an absorption edge, the DAS technique cannot be applied to atoms whose atomic numbers are less than 24 (Cr). As the edge energy decreases, the region of reciprocal space that is accesible to measurement becomes smaller, with the effect that the resolution of the DDF in real space is degraded. The potential of anomalous scattering experiments is not limited to obtaining DDF's. It is possible to obtain the **partial distribution function** (PDF), in which the intensities of both the central atom and its neighbors are known. The $\alpha\beta$ PDF

describes the distribution of β atoms around a central α atom; it is equal to $4\pi r^2 \rho_{\alpha\beta}(r)$, where $\rho_{\alpha\beta}(r)$ is the number density of β atoms at a distance r from an α atom at the origin. The total number $\alpha - \beta$ distances in the structure is constant, leading to the condition

$$X_\alpha \rho_{\alpha\beta}(r) = X_\beta \rho_{\beta\alpha}(r)$$

where X is the mole fraction. The RDF and the DDF's are related to the PDF's by

$$RDF = \sum_{\alpha=1}^{M} X_\alpha DDF_\alpha = \sum_{\alpha=1}^{M} X_\alpha \sum_{\beta=1}^{M} PDF_{\alpha\beta}$$

Keating demonstrated how M(M+1)/2 independent scattering experiments can be used to determine the same number of indipendent PDF's. In each experiment, the scattering factors of one or more of the components must be altered in indipendent way. The energy dependence of the anomalous scattering factors provides one means to accomplish this. If we consider a three components glass, six scattering patterns must be collected, two in the vicinity of the K absorption edge of each component. The PDF's are difficult to obtain because the independence that can be achieved by varying the anomalous scattering factors is limited. In practice, the results are very sensitive to experimental error.

2.1 Anomalous scattering factors

The X-ray scattering factor of an atom is the amplitude and phase of the wave scattered coherently from the atom relative to the amplitude and phase of the wave scattered by an isolated, or free, electron. In general, the atomic scattering factor f is complex and is written as

$$f = f_0(h) + f'(h, E) + if''(h, E)$$

which explicitly states the dependences on E, the X-ray energy, and h, the magnitude of the scattering vector:

$$h = \frac{4\pi \sin\theta}{\lambda}$$

where 2θ is the scattering angle, and λ is the X-ray wavelength. The quantity f_0 is the scattering factor when the X-ray energy is much greater than the largest ionization energy for the atom. At such energy, all electrons in the atom scatter as if they where free. If the X-ray energy is comparable to or less than the ionization energies of some of the electrons, the ASF's f' and f'' are nonzero. The ASF's correct the amplitude and phase of f_0 for the fact that these electrons do not scatter as free electrons. Values for f_0 have been calculated from theory for isolated atoms and ions. The anomalous scattering factors can be calculated theoretically or determined experimentally. The ASF's determined

theoretically (see Fig.16) are quite accurate when the X-ray energy is not close to an absorption edge. However, in the immediate vicinity of the edge, solid state effects cause significant deviations from the isolated atom results. The ASF's used in DAS experiments, therefore, should be measured experimentally.

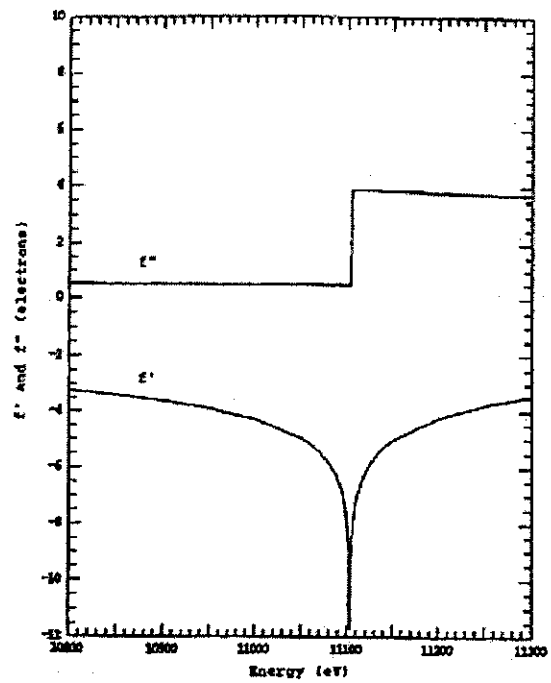

Figure 16: Cromer and Liberman calculation of the ASF's for Ge near the Ge L Absorption Edge (11103 eV).[10]

The method commonly employed for DAS experiments is to use the optical theorem to calculate f'' from a measurement of the absorption cross section as a function of energy; f' is calculated from f'' via the Kramers-Kronig relation. The optical theorem can be derived by relating the composite effect of the scattering by individual atoms in a substance to the complex index of refraction characterizing the material as a whole. The imaginary part of the index of refraction corresponds to the absorption of a wave as it travels in the material and can be expressed in terms of the total absorption cross section σ. The

optical theorem relates f'' to σ:

$$f''(\omega) = \frac{mc\omega\sigma(\omega)}{4\pi e^2}$$

where f'' is in electrons, σ has units $cm^2/atom$, m and e are the mass and charge of an electron, ω the X-ray angular frequency, and c the speed of light; all units are cgs. The Kramers-Kroning relation is

$$f'(\omega) = \frac{2}{\pi}\int_0^\infty \frac{\omega f''(\omega)}{\omega_0^2 - \omega^2} d\omega$$

in which the integral is understood to be the Cauchy principal value.

2.2 RDF Analysis

Under the assumptions of the kinematic theory of X-ray diffraction, the coherently scattered intensity in electron units (eu) from a collection of atoms is

$$I_{eu}(\mathbf{h}) = \sum_i \sum_j f_i^* f_j exp(i\mathbf{h}\cdot\mathbf{r_{ij}}) \tag{16}$$

where the summations over i and j are for all atoms in the sample, $\mathbf{h}$ is the scattering vector, $\mathbf{r_{ij}}$ the vector from atom i to atom j, and the asterisk denotes the complex coniugate. The scattering is uniform with respect to sample orientation. Therefore, after taking the spherical average of the experimental term, separating the indipendent scattering (i=j) terms, and grouping the distances between two specific types of atoms together, the equation can be rewritten as

$$I_{eu}(h) = \sum_{\alpha=1}^{M} N_\alpha |f_\alpha|^2 + \sum_{\alpha=1}^{M}\sum_{\beta=1}^{M} f_\alpha^* f_\beta \sum_i \sum_j \frac{\sin(hr_{ij})}{hr_{ij}} \tag{17}$$

in which α and β refer to kinds of atoms in an M component system, i and j are now summations over the α and β types respectively, and N_α is the number of α atoms. Next, the continuous partial density function $\rho_{\alpha\beta}(r)$ is defined in terms of the discrete interatomic distances present in the structure:

$$4\pi r^2 \rho_{\alpha\beta}(r) dr = \frac{1}{N_\alpha}\sum_{i=1}^{N_\alpha}\sum_{j=1}^{N_\beta} \delta(r - r_{ij}) \tag{18}$$

Here, δ is the delta function. At large radii $\rho_{\alpha\beta}(r)$ approaches the average density of b atoms $\rho_{\beta 0}$. Equation (18) is introduced into eq.(17) as the average density $\rho_{\beta 0}$ and the deviation from that density $\rho_{\alpha\beta}(r) - \rho_{\beta 0}$. Warren showed that the contribution from the average density is only significant at small scattering angles, where the intensity is not experimentally measured. The result, neglecting the small angle scattering term, is

$$I_{eu}(h) = \sum_{\alpha=1}^{M} N_\alpha |f_\alpha|^2 + \sum_{\alpha=1}^{M}\sum_{\beta=1}^{M} N_\alpha f_\alpha^* f_\beta \int_0^\infty 4\pi r^2 [\rho_{\alpha\beta}(r) - \rho_{\beta 0}] \frac{\sin(hr)}{hr} dr \tag{19}$$

Defining the partial structure factor as

$$S_{\alpha\beta}(h) = \frac{1}{h}\int_0^\infty 4\pi r[\rho_{\alpha\beta}(r) - \rho_{\beta 0}]\sin(hr)dr \tag{20}$$

and utilizing $N_\alpha\rho_{\alpha\beta} = N_\beta\rho_{\beta\alpha}$ to group dependent density functions together, Eq(19), on a per-atom basis now, becomes

$$I_{eu}(h) - \langle|f^2|\rangle = \sum_{\alpha=1}^{M}\sum_{\beta=\alpha}^{M} X_\alpha T_{\alpha\beta} Re[f_\alpha^* f_\beta] S_{\alpha\beta}(h) \tag{21}$$

where the brackets $\langle\rangle$ denote the molar average, X is the molar fraction and $T_{\alpha\beta}$ equals 2 when $\alpha \neq \beta$ and 1 otherwise.

This is the basic equation for amorphous scattering. It breaks the observed scattering pattern into the coherent independent scattering from individual atoms and the structure-dependent scattering due to distance correlations between atoms. The latter is expressed as the weighted sum of M(M+1)/2 independent partial structure factors.

The present development has assumed that I_{eu} is the intensity of the coherent scattering. Experimentally, I_{eu} could contain Compton scattering as well. In that case, the Compton scattering must be subtracted from I_{eu}. If only one scattering pattern is available, no basis exists for distinguishing the separate contributions of the partial structure factors to the total pattern. Let us treat the pattern as if it originated from a structure consisting of identical "average" atoms. The scattering factor of these fictitious atoms will be taken as $\langle|f|\rangle$. By analogy with eq. (21), we write

$$I_{eu}(q) - \langle|f^2|\rangle = \langle|f|\rangle^2 S(h) \tag{22}$$

where, with reference to eq.(20), the total structure factor S is related to the real space structure by

$$S(h) = \frac{1}{h}\int_0^\infty 4\pi r[\rho(r) - \rho_0]\sin(hr)dr \tag{23}$$

In effect, eqs. (22) and (23) define S(h) and $\rho(r)$. From eq. (23), it is apparent that the two functions are related by a Fourier sine transform. After obtaining S(h), from experimental data using eq.(22), the reduced RDF, G(r), is calculated as

$$G(r) = 4\pi r[\rho(r) - \rho_0] = \frac{2}{\pi}\int_0^\infty hS(h)\sin(hr)dh \tag{24}$$

From G(r), the radial density function $\rho(r)$ and the RDF $4\pi r^2\rho(r)$ can be obtained. The reduced RDF of a multicomponent system describes the structure in terms of fictitious atoms, which are defined by the average atomic scattering factor. The relationship of G(r) to the $\rho_{\alpha\beta}(r)$'s, which describe the correlations of the actual atoms in the structure, becomes clear by equating eq.(20) to

eq.(21) and Fourier transforming. The result is

$$G(r) \approx \sum_{\alpha=1}^{M} \sum_{\beta=\alpha}^{M} X_\alpha T_{\alpha\beta} \frac{Z_{eff,\alpha} - Z_{eff,\beta}}{\langle Z_{eff} \rangle^2} G_{\alpha\beta}(r) \tag{25}$$

in which $Z_{eff} = Z + f'$, Z being the atomic number. The reduced PDF is defined as

$$G_{\alpha\beta}(r) = 4\pi r[\rho_{\alpha\beta}(r) - \rho_{\beta 0}] = \frac{2}{\pi} \int_0^\infty h S_{\alpha\beta}(h) \sin(hr) dh \tag{26}$$

According to eq.(25), G(r) contains contributions from each $G_{\alpha\beta}(r)$, weighted according to the composition and the scattering abiliyt of the atoms involved.

2.3 Anomalous SAXS Applications to Catalysts

This lesson is based on the Reference [57].

2.3.1 Introduction

Heterogeneous catalysis deals with the transformation of molecules at the interface between a solid (the catalysts) and the gaseous or liquid phase which carries these molecules [16]. Consequently quantitative characterization of these systems, concerning both the exposed surface and the bulk structure, is a matter of obvious importance in understanding the mechanisms of the chemical reactions and in developing new catalysts with higher performance. Moreover, although most practical catalysts are highly complex materials, it has been widely shown that their catalytic activity can be affected by their microstructure. The most common technique employed to characterize catalysts is the selective chemisorption of a suitable gas onto the surface of the active component, though this technique is generally of little use for non metallic catalysts. The other major methods are based on X-ray diffraction, photoelectron spectroscopy and electron microscopy [17], [18]. Obviously, any of the above-cited techniques is affected by its own limitations. For example, the adsorption stoichiometry (the average number of surface metal atoms associated with the adsorption of each adsorbate molecule) used for chemisorption measurements is not always well defined. X-ray line broadening analysis gives the size of the crystallites (very often not coinciding with the particles) larger than 1.5nm. Also, electron microscopy has its drawbacks: the micrographs can be affected by artifacts or do not give an exhaustive picture of the sample and so on.

For all these reasons, in principle SAS could be very advantageous, since it does not require a knowledge of the crystal structure of the scattering particles to determine their size, and an experiment can sample all the particles in a specimen. Moreover, industrial heterogeneous catalysts are utilized in the form of pellets, extrudates and spheres of some millimeters in size, but they are manufactured as a powder. Consequently, they can be analyzed, without any problems, by any SAS set-up used in an ordinary research laboratory.

2.3.2 Supported Metal Catalysts

Supported metal catalysts are of particular interest for a variety of reactions involving hydrogen, such as hydrogenation, hydrogenolysis and catalytic reforming. They are mostly composed of an active phase (metal), responsible for the principal chemical reaction, and a support, or carrier. Generally, the metal is highly dispersed on the support in aggregates so small that many of the atoms present are on the surface. A proper interpretation of heterogeneously catalyzed reaction kinetics requires a precise knowledge of this number of active atoms, exposed on the surface, or, more precisely, of the value of dispersion. The dispersion of the active fraction of a catalyst is defined by the ratio between the number of the active atoms exposed at the surface and the total number of active atoms present in the catalyst. For systems, where the active fraction is

present as separate particles, distinguishable from the carrier and characterized by definite shape, simple relationships can be found among the dispersion, the surface area and the size of the active particles.

Supports Before talking about catalysts, a short summary of the SAS studies on supports will be given here. Supports, or carriers, perform many functions, but the most important is the maintenance of a high surface area for the active component. High area supports commonly used in catalyst manufacturing are activated carbon, active alumina, amorphus silica gel, zirconia, clays, titania and magnesia.

Some of these porous solids have been the object of extensive SAS literature. For example, I would like to mention all the papers concerning the fractal properties of some of these systems published in these last few years [19], [20]. However, a description of these results is beyond the aim of the present paper, even if these works can give useful information on the preparation of good supports.

Instead, I will focus mostly on the fact that SAS can provide useful information on the pore structure and surface area measurements of these systems. Usually, N_2 adsorption isotherms are widely used to obtain these microstructural features, but when a microporous structure with closed pores is analyzed, this technique is incapable of measuring the whole surface of the pores [21]. Generally, the scattering curves of amorphous silica gel, active alumina and zirconia display a well-developed high angle region, where the slit-smeared intensities vary as h^{-3} (Porod's law region) [22], [23], [24]. Nevertheless, the study of some supports, in particular activated carbon with a high surface area, is usually complicated by the presence of a continuous positive deviation from the Porod's law of the scattering intensity. This experimental evidence has induced researchers to develop new approaches [19], [25], perhaps less "traditional", as far as the measure of specific surfaces is concerned, but still providing a physical picture of the porous structure.

Some porous materials, which are sometimes used as supports, are also good catalysts. A typical example are pillared clays used as cracking catalysts, capable of converting heavy oil fractions containing large refractory molecules. Pillared clays generally present textural complexity, geometrical constraints and possible chemical heterogeneity induced by pillaring. As far as surface area and porosity measurements by physical adsorption of nitrogen are concerned, this overall complexity introduces difficulties in interpretation. Moreover, suitable methods of preparation can be used to tailor the pore sizes. However, in spite of the extensive literature, the contribution, to the knowledge of the texture of these porous materials given by SAS measurements is very poor [26].

Catalysts One major practical difficulty with an SAS investigation of supported metal catalysts is that they are three-phase systems. Consequently, the porous structure of the support can produce a parasitic scattered intensity which can interfere with the scattering from metal particles.

Two main approaches have been developed to overcome this difficulty. The first one was aimed at reducing the magnitude of the void scattering through some experimental procedures. Gunn [27] found that the scattering from micropores of a silica-alumina cracking catalyst could be eliminated by the sorption of liquids with electron densities very close to those of the support. This procedure, known as the pore-maskant method, has been used in some SAXS laboratories [28], [29], [30], [31], [32], but it is limited by the fact that the imbibition liquids may affect the catalyst in unknown ways, and it is difficult to assure reproducibility in filling the pores. Nevertheless, this is the only method that can be used for the study of many metal catalysts, which are mostly supported on activated carbons or active aluminas since the scattering intensity of the catalyst, due to the interference phenomena between pores and metal particles, shows different features from the support intensity. The intensities thus obtained can be used to determine the average particle sizes and/or the particle size distribution N(d) (d=characteristic dimension of the particle). Usually, the size distribution of metallic particles of supported catalysts are log-normal-like [33]. This is related to the growth of the particle in accordance with a coalescence mechanism. Basically, there are three methods of evaluating N(d). The first one assumes a simple distribution function for N(d) which contains only a few parameters, which can be evaluated from the measured intensity [34]. The second one determines N(d) by numerical analysis methods without any assumption as to the form of the distribution [35], [36], [37]. The third one is based on the Fourier tranform of the scattered intensities [38], [39], [40].

A different procedure was proposed by Somorjai et al. [41]. With this method which, however, is no longer applied, the porous structure was compressed at very high pressure, in order to convert the catalyst into a two-phase system. The second method is theoretical, and proposes a model based on some physical assumptions in order to calculate also the metal-void surface area or the particle size distribution of the metal phase. The simplest way to proceed, when interference effects are absent, is to consider as additive the scattering due to the different phases present in the system. Using this hypothesis, the effect due to the porous support is subtracted from the total scattering curves after their normalization on the same scale. After the subtraction the intensities can provide the same parameters obtained with the pore maskant method.

Although some empirical relationships between the phases had been proposed [42], a significant contribution to the theoretical approach was made by Brumberger and Goodisman [43], [44], [22]. In 1981 they first proposed, on the assumption that the introduction of the metal reduces the pore space in direct proportion to the increase in the metal, a method which is able to determine numerical values for the specific surfaces between metal and support and metal and vacuum, from only two separate experiments on the catalyst and the support. This idea has been further developed in some other papers, using some other physical assumptions [45], or different functional parametrizations of the scattered intensity [46]. Finally, new models based on the concept of Voronoi cells [47], [48], [49], [50], [23] have been proposed. All this work is very important: first, because it shows the great potential of SAS in the study of

catalysts and second, because it makes available, to the researchers involved in catalysis, a very powerful method of investigating the microstructural properties of these systems. Usually, the data reported in the literature show a fairly good agreement between SAS and other techniques [30], [42], [32]. As expected, the average size of the metallic particles calculated by SAS is larger than the crystallite size obtained by WAXS. Meanwhile, the agreement with the chemisorption and TEM results is sometimes strongly related to the type of catalyst investigated [51], [52], [53].

Finally, I will make some comments about the use of synchrotron radiation, as a possible improvement of SAS studies on supported metal catalysts. It is well known that, by tuning the incident photon energy close to the absorption edge of an element, in our case a metal, its atomic scattering amplitude can be varied. Since the scattering due to the support does not change appreciably for small changes in photo energy, the difference between two scattering intensities measured at a photon energy very near the metal absorption edge, and at some tens of eV away, can give the scattering due to the metal particles alone. This kind of approach has already been successfully applied to some Pt catalysts supported on silica gels and alumina using wide-angle X-ray scattering measurements [54]. Recently, this approach known as Anomalous Small Angle X-ray Scattering (SAXS) has been applied to a series of metal supported catalysts containing Au and Pd supported on active carbon and silica and measuring strategies were optimized in order to obtain reliable results [55], [56]. The results seem to be very promising since we have been able to detect also small nanoclusters (size of about 2nm) which remained undetected until now.

References

[1] L. V. Azaroff and M. J. Buerger, The Powder method (1958). Mac Graw Hill, New York.

[2] B. E. Warren, X-Ray Diffraction (1969). Addison-Wesley, Reading.

[3] H. P. Klug and L. E. Alexander, X-Ray diffraction procedures (1974). Wiley, New York.

[4] A. Guinier, X-Ray Diffraction (1963). Freeman, San Francisco.

[5] C. Giacovazzo, H. L. Monaco, D. Viterbo, F. Scordari, G. Gilli, G. Zanotti and M. Catti, Fundamental of Crystallography (1992). Oxford Science Pubblication, Oxford.

[6] R. A. Young The Rietveld Method (1993) Edited by R.A.Young, Oxford Science Publications, Oxford.

[7] R. I. Smith, A. R. West, I. Abrahams and P.G.Bruce, Powder Diffr. (1990), 5, 137.

[8] C.N.J.Wagner, M.S.Boldrick and L.Keller, Adv.X-Ray Analysis (1988), 31, 129.

[9] G.Lim, W.Parrish, C.Ortiz, M.Bellotto and M.Hart, J.Mater.Res. (1987), 2, 471.

[10] J.D.Westwood, Ph.D. thesis, Northwestern University, June 1988 .

[11] Y.Waseda, Novel Application of Anomalous (Resonance) X-ray Scattering for Structural Characterization of Disordered Materials (1984). Springer-Verlang, Berlin.

[12] N.J.Shevchik, Phil.Mag. (1977), 35, 805.

[13] N.J.Shevchik, Phil.Mag. (1977), 35, 1289.

[14] P.H.Fuoss, W.K.Warburton,and A.Bienenstock, J.Non-Cryst. Solids (1980), 35-36, 1233.

[15] P.H.Fuoss, P.Eisenberger, W.K.Warburton,and A.Bienenstock, Phys.Rev.Lett. (1981), 46, 1537.

[16] Delannay F. & Delmon, B. (1984).Characterization of heterogeneous Catalysis, edited by F.Delannay, pp.1-28. New York: Marcel Dekker.

[17] Lemaitre, J.L., Menon, P.G. & Delannay F. (1984).Characterization of heterogeneous Catalysis, edited by F.Delannay, pp.299-365. New York: Marcel Dekker.

[18] Matyi, R.J., Schwartz, L.H. & Butt, J.B., (1987). Catal. Rev.-Sci.Eng. 29, 41-99.

[19] Schmidt. P.W. (1990). The fractal approach to heterogeneous Chemistry, edited by D.Avnir, pp.67-78. Chichester, England: Wiley.- Papers presented at VIII and IX International Conference on Small Angle Scattering and published respectively in J.Appl.Cryst. (1991) vol. 24 and in J.de Phys. (1993), 3 Colloque 8.

[20] Benedetti, A., Fagherazzi, G., Riello, P. Zeng,Y.W., Pinna, F. & Signoretto M. (1993). J.Appl.Cryst. 26, 717-720.

[21] Ruike, M., Kasu, T., Setoyama, N., Suzuki, T. & Kaneko, K., (1994). J.Phys.Chem. 98, 9594-96007) -

[22] Goodisman, J., Brumberger, H. & Cupelo, R. (1981). J.Appl.Cryst. 14, 305-308.

[23] Brumberger, H., Delaglio, F., Goodisman, J. & Whitfield (1986). J.Appl.Cryst. 19, 287-299.

[24] Floriano, M., Venezia, A.M., Deganello, G., Svensson, E.C. & Root, J.H. (1994). J.Appl.Cryst., 27, 271-277.

[25] Ciccariello S., Benedetti, A. and Polizzi S., (1991). J.Appl.Phys. 69, 6355-6359.

[26] Pinnavaia, T.J., Rainey, V., Ming-Shing Tzou & White, J.W., (1984). J.Mol.Catal. 27, 213-234.

[27] Gunn, E. (1958). J.Phys.Chem. 62, 928-934

[28] White, T.E.Jr., Kirklin, P.W., Gould, R.W, & Heinemann, H. (1972), J.Catal. 25, 407-415.

[29] Renouprez, A. & Imelik, B. (1973), J.Appl.Cryst. 6, 105-113.

[30] Renouprez, A., Hoang-Van, C. & Compagnon, P.A. (1974). J. Catal. 34, 411-422.

[31] Cocco, G., Enzo, S, Fagherazzi, G., Schiffini, L., Bassi, I.W., Vlaic, G., Galvagno, S. & Parravano, G. (1979). J.Phys. Chem. 83, 2527-2538.

[32] Lopez, T., Asomoza, M., Bosch, P., Garcia-Figueroa, E. & Gomez, R. (1992). J.Catal. 138, 463-477.

[33] Granquist, C.G. & Buhrman, R.A. (1976). J.Catal. 42, 477-479.

[34] Baur, R. & Gerold, V. (1964). Acta Metall. 12, 1448-1453.

[35] Vonk, C.G. (1976). J.Appl.Cryst. 9, 433-440.

[36] Glatter, O. (1977). J.Appl.Cryst. 10, 415-421.

[37] Svergun, D.I., Semenyunk, A.V. & Fegin, L.A. (1988). Acta Cryst. A44, 244-250.

[38] Fedorova & Schmidt P.W. J.Appl.Cryst.

[39] Mering J.& Tchoubar, D. (1968). J.Appl.Cryst. 1, 153-165.

[40] Brusset, H. & Donati, J.R. (1969). J.Appl.Cryst. 2, 55-62.

[41] Somorjai, G.A., Powell, R.E., Montgomery, P.W. & Jura G. (1967) . Small Angle X-Ray Scattering, edited by H.Brumberger, pp.449-466.New York: Gordon and Breach.

[42] Fagherazzi, G., Cocco, G., Schiffini, L., Enzo, S., Benedetti, A., Passerini, R., & Tauszik, G.R. (1978). Chim.Ind. 60, 892-900.

[43] Goodisman, J. & Brumberger, H. (1971). J.Appl.Cryst. 4, 347-351.

[44] Goodisman, J. & Brumberger, H. (1979). J.Appl.Cryst. 12, 398-399.

[45] Espinat, D., Moraweck, B., Larue, J.F. & Renouprez, A.J. (1984). J.Appl.Cryst., 17, 269-272.

[46] Ciccariello, S., & Benedetti, A. (1985). J.Appl.Cryst. 18, 219-229.

[47] Goodiman, J. & Coppa, N. (1981). Acta Cryst. A37, 170-180.

[48] Coppa, N. & Goodisman, J. (1981). J.Appl.Cryst. 14, 309-314

[49] Brumberger, H. & Goodisman, J. (1983). J.Appl.Cryst. 16, 83-88.

[50] Brumberger, H., Chang, Y.C., Phillips, M.G., DeLaglio, F. & Goodisman, J. (1986). J.Catal. 97, 561-564.

[51] Polizzi, S., Benedetti, A., Fagherazzi, G., Franceschin, S., Goatin, C., Talamini, G. & Toniolo, L. (1987). J.Catal.,106, 483-497.

[52] Fagherazzi, G., Benedetti, A., Deganello, G., Duca, D., Martorana, A. & Spoto, G. (1994). J.Catal., 150, 117-126.

[53] Fagherazzi, G., Benedetti, A., Polizzi, S., Di Mario, A., Pinna, F. & Pernicone, N. (1995). Catal. Lett., 32, 293-303.

[54] Georgopoulos, P. & Cohen, J.B. (1985). J.Catal. 92, 211-215.

[55] Benedetti, A., Polizzi, S., Riello,P., Pinna, F., Goerigk, G. (1997) . J Catal. 171, 345-348.

[56] Benedetti, A., Bertoldo, L., Canton, P., Goerigk, G., Pinna, F., Riello, P., Polizzi, S. (1999). Cat.Today 49, 485-489.

[57] Benedetti, A. (1997) J. Appl. Cryst. 30, 647-652.